



CHORUS

This is the accepted manuscript made available via CHORUS. The article has been published as:

Anomalous Hall effect at the Lifshitz transition in ZrTe_5

P. M. Lozano, Gabriel Cardoso, Niraj Aryal, D. Nevola, Genda Gu, Alexei Tsvetik, Weiguo Yin, and Qiang Li

Phys. Rev. B **106**, L081124 — Published 29 August 2022

DOI: [10.1103/PhysRevB.106.L081124](https://doi.org/10.1103/PhysRevB.106.L081124)

Anomalous Hall effect at the Lifshitz transition in ZrTe_5

P. M. Lozano,^{1,2,*} Gabriel Cardoso,^{1,*} Niraj Aryal,² D. Nevola,²
Genda Gu,² Alexei Tsvelik,² Weiguo Yin,² and Qiang Li^{1,2,†}

¹*Department of Physics and Astronomy, Stony Brook University, Stony Brook, New York 11794-3800, USA*

²*Condensed Matter Physics and Materials Science Division,
Brookhaven National Laboratory, Upton, New York 11973-5000, USA*

(Dated: August 22, 2022)

Zirconium pentatelluride ZrTe_5 is a topological semimetal. The presence of a temperature induced Lifshitz transition, in which the Fermi level goes from the conduction band to the valence band with increasing temperature, provides unique opportunities to study the interplay between Fermi-surface topology, dynamics of Dirac fermions, and Berry curvature in one system. Here we present a combined experimental and theoretical study and show that a low energy model can be used to understand the complicated Hall response and large anomalous Hall effect observed in ZrTe_5 over a wide range of temperature and magnetic field. We found that the the anomalous Hall contribution dominates the Hall response in a narrow temperature window around the Lifshitz transition, away from which the orbital contribution dominates. Moreover, our results indicate that a topological phase transition coexists with the Lifshitz transition. Our model provides a unifying framework to understand the Hall effect in semimetals with large Zeeman splitting and non-trivial topology.

Zirconium pentatelluride ZrTe_5 lies at the boundary between a strong and a weak topological insulator, where the gapless state corresponds to a Dirac semimetal [1–7]. The non-trivial topology of electronic bands and dynamics of Dirac fermions in ZrTe_5 have generated considerable attention recently by bringing together chiral magnetic effect [8], three-dimensional quantum Hall effect [9], and anomalous Hall effect (AHE) [10–12] in a single material. Recent ultrafast terahertz experiments have found giant dissipationless chiral photocurrent arises at the temperature where AHE was detected in the same ZrTe_5 single crystals [6, 13].

In non-magnetic materials, such as ZrTe_5 and Cd_3As_2 , the AHE is generally attributed to the intrinsic Berry curvature of the electronic bands [14, 15]. ZrTe_5 has a large Zeeman splitting with Landé g -factor of ~ 21 , which in turns produces a large AHE [11, 16–18]. Another distinctive feature of ZrTe_5 is its anomalous resistivity peak at temperature T_p (≈ 75 K in our sample), shown in Fig. 1(a). The resistive anomaly has its origin in the temperature induced Lifshitz transition, in which the Fermi level goes from the conduction to the valence band with increasing temperature [19–28] and can be understood in the following way. As the Fermi level approaches the small band gap, the density of states is reduced and thus conductivity is suppressed. This behavior is schematically shown in the left insets of Fig. 1(a), while Fig. 1(b) shows the actual band dispersion taken by angle-resolved photoemission spectroscopy (ARPES) at different temperatures on samples used in the resistivity measurements. The ARPES data were taken along a momentum cut parallel to the conducting chain axis, the crystallographic a -axis, with incident photon energy of 6 eV and an overall resolution of 4meV [29].

The large Zeeman splitting, the strong Berry curvature, and the presence of a temperature induced Lif-

shitz transition produce a complicated temperature and magnetic field dependence of the Hall response in ZrTe_5 , shown in 1(d), and it is poorly understood. To understand this, we performed a combined experimental and theoretical study to investigate various factors that contribute to the Hall response. Using a low energy model, we quantify the Berry curvature contribution and the orbital contribution to the Hall response as a function of magnetic field at different temperatures. We identified that the Berry curvature makes the dominant contribution to the Hall response in the vicinity of the Lifshitz transition, where the orbital contribution is significantly smaller due to the reduced density of states. Far away from the Lifshitz transition, the orbital contribution dominates the Hall response, while the contribution from the Berry curvature induced AHE is subdued. This low energy analytical model reconciles various observations in ZrTe_5 .

Experimentally, the transport properties of ZrTe_5 were investigated with the current applied along the a -axis of the single crystals and the magnetic field applied parallel to the crystallographic b -axis, which is the z axis in the insets of Fig. 1(b,d) [29]. Both the longitudinal resistivity ρ_{xx} and Hall resistivities ρ_{yx} are measured as a function of magnetic field at various temperatures, and they are shown in Fig. 1 (c,d). In the high field regime, the Hall resistivity becomes non-linear, signaling the presence of the AHE. This AHE was observed at temperatures as high as 190 K, which coincides with the onset temperature at which the light induced chiral current was observed in the same samples [13]. The non-linear contribution to the Hall response gets stronger as temperature decreases. Notably, there is a sign change in the Hall coefficient as the temperature goes through the Lifshitz transition, corresponding to the dominant charge carriers type changing from electron-like to hole-like.

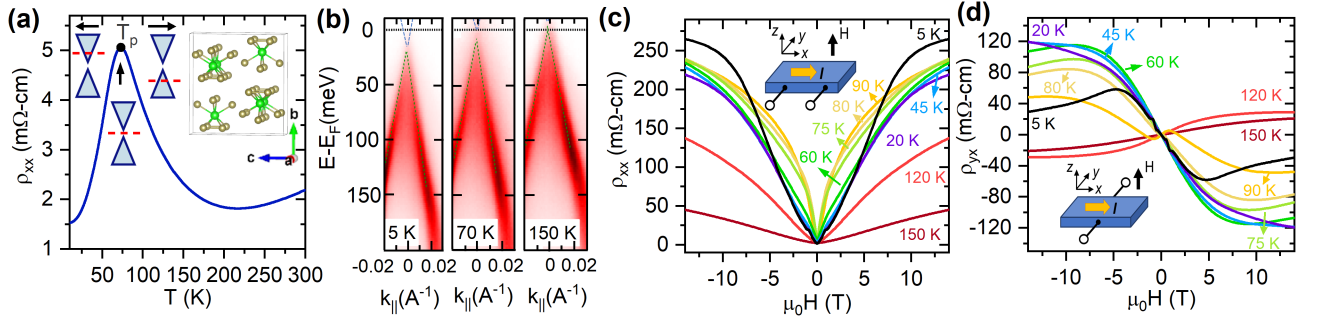


FIG. 1. (a) Temperature dependence of the longitudinal resistivity of ZrTe₅ along the a-axis. The resistivity peak at $T = T_p$ marks the temperature induced Lifshitz transition. (b) The ARPES of the dispersion near the Γ point at 5 K, 70 K and 150 K. The 70K and 150K data were divided by the Fermi-Dirac function to make the data near the Fermi level clearer, the dotted lines are guides for the eye. (c,d) Longitudinal and transverse magnetoresistivity across the Lifshitz transition. The insets show the measurement configurations.

To understand the complicated temperature and magnetic field dependence of Hall response in ZrTe₅, we investigate the Hall conductivity, which can be directly compared with theoretical predictions. The Hall conductivity can be calculated from the magnetoresistivity measurements via the relation $\sigma^{xy} = \rho_{yx}/(\rho_{xx}^2 + \rho_{yy}^2)$ [30]. The total measured Hall conductivity consists of two contributions, the orbital one and the anomalous one, $\sigma^{xy} = \sigma_{\text{orbital}}^{xy} + \sigma_{\text{AHE}}$ [14], where the orbital contribution $\sigma_{\text{orbital}}^{xy}$ comes from the Drude formula [31]

$$\sigma_{\text{orbital}}^{xy} = \frac{en\mu^2 B}{1 + \mu^2 B^2}. \quad (1)$$

In the low field limit, $\sigma_{\text{orbital}}^{xy} \sim B$, while in the high field limit, $\sigma_{\text{orbital}}^{xy} \sim 1/B$. The maximum value of $\sigma_{\text{orbital}}^{xy}$ occurs at $B = \mu^{-1}$. Given the high mobility $\mu \sim 10^5$ cm²/Vs in ZrTe₅, the maximum $\sigma_{\text{orbital}}^{xy}$ appears at $B \sim 0.2$ T. The overall magnitude of $\sigma_{\text{orbital}}^{xy}$ depends on the carrier density n . Fig. 2(a) shows the magnetic field dependence of the calculated $\sigma_{\text{orbital}}^{xy}$ in ZrTe₅ at three different temperatures.

Now, we turn to the anomalous contribution to the total Hall conductivity, σ^{xy} , which is given by the sum of the Berry curvature over the occupied states,

$$\sigma_{\text{AHE}} = \frac{e^2}{\hbar} \sum_n \int \frac{d^3k}{(2\pi)^3} f(E^n, \mu, T) \Omega_z^n, \quad (2)$$

where Ω_z^n is the z component of the Berry curvature of band n , f is the Fermi-Dirac distribution and μ is the chemical potential. Since the Berry curvature is concentrated at the Γ point, which the Fermi level lies close to, it is natural to start with a linearized low energy model of the Hamiltonian. We do this by using the $k \cdot p$ model of Chen *et al.* [32], consistent with the symmetries of ZrTe₅,

$$H_0 = m\tau^z + \hbar(v_x k_x \tau^x \sigma^z + v_y k_y \tau^y + v_z k_z \tau^x \sigma^x), \quad (3)$$

where m is the effective mass of the Dirac fermions, v_i and k_i are the i -th components of the Fermi velocity and crystal momentum, respectively, and σ and τ represent the

spin and orbital degrees of freedom, respectively. Given the large Zeeman splitting in ZrTe₅, the main effect of an external magnetic field can be incorporated by including the Zeeman energy term $H_Z = g\mu_B B \sigma^z/2$ in the total Hamiltonian. In this linear approximation, the energies and Berry curvatures of the four bands are given by

$$E^{s_1 s_2} = s_1 \sqrt{(b + s_2 \sqrt{m^2 + k_{\perp}^2})^2 + k^2}, \quad (4)$$

$$\Omega_z^{s_1 s_2} = -s_2 \frac{m}{2(m^2 + k_{\perp}^2)^{3/2}}, \quad (5)$$

where the s_i are \pm signs labeling the four bands and the parametrization in energy units $b = g\mu_B B/2$, $k = \hbar v_z k_z$ and $k_{\perp} e^{i\phi} = \hbar(v_x k_x + i v_y k_y)$ was adopted. The details of this calculation can be found in [29]. Eq.(5) is well-known for the case of a band crossing in 2D systems. Here it shows that the Berry curvature of the four bands in ZrTe₅ is constant along k_z . On a given k_z slice, there is a Chern number-like relation

$$\int k_{\perp} dk_{\perp} d\phi \Omega_z^{s_1 s_2} = -\pi s_2. \quad (6)$$

This Berry curvature is concentrated on a region of size m around $k_{\perp} = 0$. In the limit $m \rightarrow 0$, $\Omega_z^{s_1 s_2} \rightarrow -\pi s_2 \delta(k_{\perp} e^{i\phi})$. Fig. 2(c) shows the calculated band structure and the value of the z component of the Berry curvature at various magnetic fields.

The magnetic field dependence of the anomalous Hall contribution from Eq. (2) can be understood as follows. At zero field, the valence and the conduction band are each doubly degenerate. The Berry curvature of the degenerate bands have equal magnitude but opposite sign that cancel out each other completely, as shown on the left of Fig. 2(c). This leads to zero Berry curvature everywhere in the Brillouin zone, resulting in no AHE. When a magnetic field is applied, the degeneracy is lifted leading to a non-zero Hall contribution from the Berry curvature.

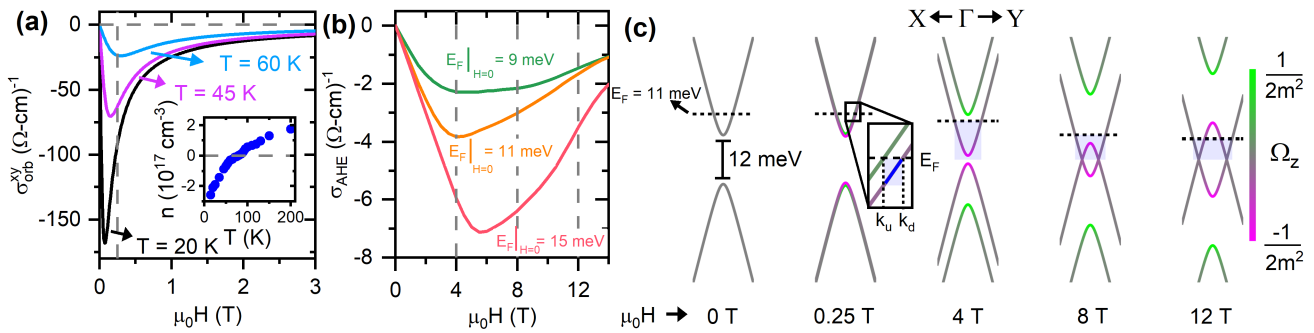


FIG. 2. **(a,b)** Magnetic field dependence of the calculated $\sigma_{\text{orbital}}^{xy}$ below T_p for several temperatures and the calculated σ_{AHE} for different zero field Fermi levels of ZrTe_5 , respectively. The charge carrier density n shown in the inset plot of (a). **(c)** The calculated electronic band structure of ZrTe_5 near the Γ point, together with the calculated z component of the Berry curvature Ω_z , (values shown in the color scale), the dotted line represents the position of the Fermi level.

The anomalous Hall conductivity is then given by

$$\sigma_{\text{AHE}} = \frac{e^2}{\hbar} \int \frac{dk_z dk_{\perp}}{(2\pi)^3} (f^{++} - f^{+-} + f^{-+} - f^{--}) \times \frac{-mk_{\perp}}{2(m^2 + k_{\perp}^2)^{3/2}}, \quad (7)$$

where we used the short-hand notation $f^{s_1 s_2} = f(E^{s_1 s_2}, \mu, T)$, and the magnetic field dependent chemical potential is determined by fixing the charge carrier density in the system.

For simplicity, we first consider the zero-temperature limit. In a small field (e.g. 0.25 T), the Zeeman energy splits both the conduction and valence bands into two. The split conduction bands intersect with the Fermi level E_F at k_u and k_d for the up-shifted band and down-shifted band, respectively, shown in the inset to Fig. 2(c). At the Dirac point, the Berry curvature makes effectively zero contribution to σ_{AHE} due to the opposite sign of the split conduction bands in this region. This is true for the states with $k_{\perp} \leq k_u$ on the conduction bands and is true for all the states on the valence bands. Only the states with $k_u < k_{\perp} \leq k_d$ (marked by blue in the region) effectively contribute to σ_{AHE} . As the field increases, the band splitting increases leading to a smaller value of k_u and a larger value of k_d , which gives rise to a rapid increase in σ_{AHE} . k_u vanishes when the up-shifted conduction band is above E_F at k_u (e.g. at 4 T), at which σ_{AHE} reaches its maximum value. This picture is consistent with the phenomenological use of the hyperbolic tangent to describe the AHE in ZrTe_5 as done in recent studies [11, 12] and is explained in more detail in [29]. At a higher field (e.g. 8 T), at which the Zeeman energy becomes larger than the band gap, a band crossing appears, creating a nodal line. For even higher fields (e.g. 12 T), the states with a larger Berry curvature on the up-shifted valence band edge, which is above E_F at k_u now, stop contributing to the AHE and therefore only the states close to the nodal line contribute. This leads to an accelerated decrease in σ_{AHE} with increasing mag-

netic field. The shaded regions in Fig. 2(c) represent the states that make a net contribution to the AHE. Fig. 2(b) shows the magnetic field dependence of the calculated σ_{AHE} for ZrTe_5 using Eq. (7) with different E_F values. The higher the Fermi level is in the conduction band, the higher the magnitude of σ_{AHE} , due to higher number of participating states. The peak value of σ_{AHE} moves to a higher magnetic field, because a higher Zeeman energy is needed to drive the up-shifted conduction band edge out of E_F .

Although we explained the magnetic field dependence of the Hall conductivity through the above semiclassical formulas, it is known that ZrTe_5 may reach the strong quantum limit at magnetic fields as low as 1 T [4, 8, 32]. An intuitive way of arriving at the anomalous conductivity in this case is by noting that in symmetric gauge the Landau levels correspond semiclassically to rings in the plane of the Brillouin zone normal to the field whose enclosed area is given by integer multiples of the cyclotron frequency [33]. Thus, one can immediately quantize Eq. (7) as

$$\int dk_{\perp} \frac{mk_{\perp}}{2(m^2 + k_{\perp}^2)^{3/2}} \rightarrow \sum_n \frac{m}{4(m^2 + \alpha n)^{3/2}}, \quad (8)$$

where

$$\alpha = \frac{4v_x v_y e \hbar}{g \mu_B m}. \quad (9)$$

Therefore, at zero temperature Landau level quantization is important when α is comparable to m^2 , which indeed corresponds to magnetic fields of the order of 1 T. Typically, this prescription is only valid when many Landau levels are filled, but in the $k \cdot p$ model one can show that it is also the result of evaluating the Kubo formula in the exact eigenstates of the minimal-coupled Hamiltonian, with the details provided in the supplementary materials [29]. The continuous discussion above should therefore be understood in terms of the enveloping functions of

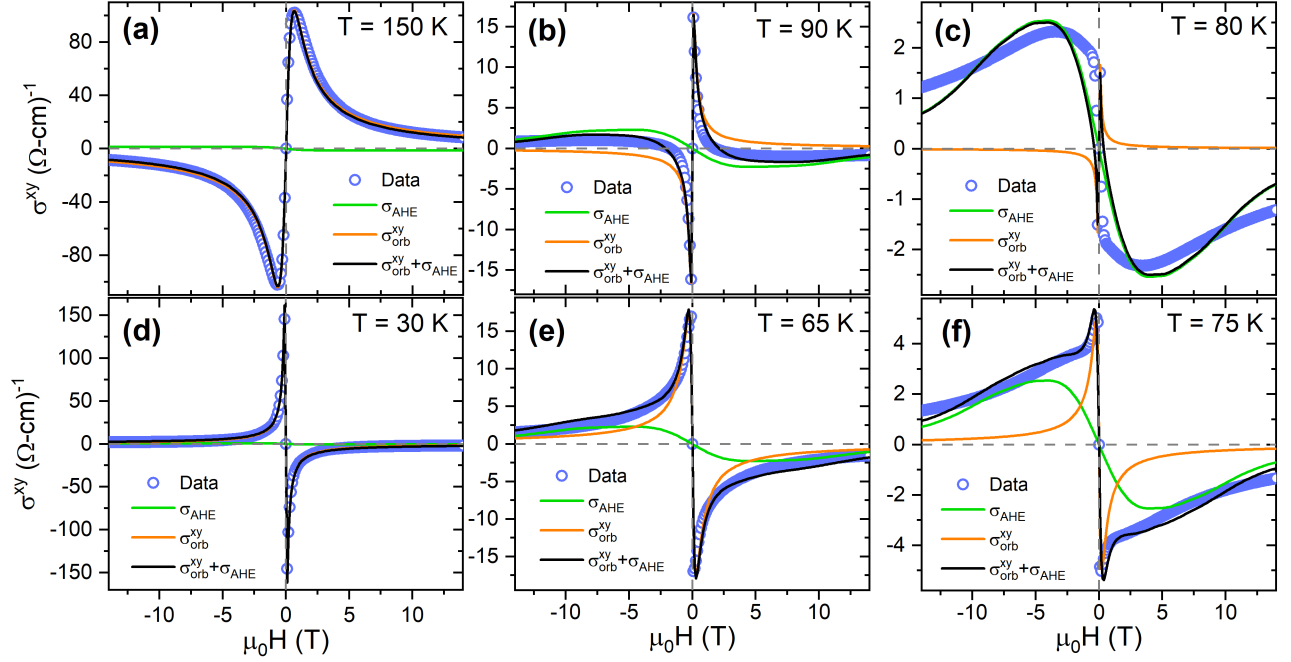


FIG. 3. Magnetic field dependence at various temperatures across the Lifshitz transition of the experimental Hall conductivity (symbols), the fitted orbital conductivity $\sigma_{\text{orbital}}^{xy}$ (orange lines), and the model prediction of the anomalous conductivity σ_{AHE} (green lines). The total Hall conductivity (black lines) comes from adding $\sigma_{\text{orbital}}^{xy}$ and σ_{AHE} . (a, d) Far from the transition the Hall conductivity is dominated by the $\sigma_{\text{orbital}}^{xy}$, overlapped with the total Hall conductivity. (b, e) As temperature moves closer to T_p , the relative contribution of the AHE increases, while $\sigma_{\text{orbital}}^{xy}$ decreases. (c, f) In close proximity to the transition, $\sigma_{\text{orbital}}^{xy}$ becomes very small in high fields, while σ_{AHE} dominates the Hall conductivity. The calculations are performed with the 3 meV Fermi level above or below the gap.

the expression for the band structure and conductivity in the presence of Landau levels.

It is known that secondary trivial bands away from the Γ point are present in ZrTe_5 . They make a negligible contribution to the Berry curvature due to their lack of coupling to any other bands [11]. As such, these trivial bands would not modify the semiclassical model for the Berry curvature induced AHE described here. **Furthermore, the secondary bands are located a few hundreds of meV away from the Fermi level, based on our ARPES characterizations of the same samples [8]. Thus, they make negligible contributions to the Hall conductivity in the vicinity of the Lifshitz transition.**

Fig. 3 shows the experimental results (symbols) and the model calculations (lines) of the magnetic field dependence of the Hall conductivity at various temperatures across the Lifshitz transition. The blue and orange lines are the orbital and the AHE contributions, respectively, to the total Hall conductivity (black lines). For $T \gg T_p$ or $T \ll T_p$, the total Hall conductivity σ^{xy} is dominated by $\sigma_{\text{orbital}}^{xy}$ derived from the classical Drude formula and σ_{AHE} is relatively negligible. This is shown in Fig. 3(a,d). Such behavior away from T_p reaffirms the validity of the proposed semiclassical model. As temperature approaches T_p , E_F approaches the band edge. $\sigma_{\text{orbital}}^{xy}$ becomes smaller due to reduced carrier density,

while the relative contribution of σ_{AHE} grows, as shown in Fig. 3(b, e). This is more clearly seen in Fig. 3(b), where the Drude formula (1) cannot explain the sign change σ^{xy} at $B \approx \pm 3$ T and the AHE contribution becomes clear.

It is quite remarkable that the dominance of the AHE in the total Hall response occurs in a narrow temperature window of ± 2 K around T_p . Fig. 3(c, f) show the Hall conductivity for $T = 80$ K and $T = 75$ K, respectively. At $T_p \approx 75$ K, the charge carriers of the system are predominantly electrons, as shown in the sign of the orbital contribution, σ_{AHE} is several times more than $\sigma_{\text{orbital}}^{xy}$ at high fields. At 80 K, the switch-over of the charge carrier types occurs, which can be seen from the positive values of the orbital contribution, where the chemical potential is expected to lie closer to the valence band edge. From 5 K to 200 K, the mobility obtained from fitting the Drude formula is in the order of 10^5 cm^2/Vs , while the carrier density n goes monotonically from $-2.5 \times 10^{17} \text{cm}^{-3}$ to $1.8 \times 10^{17} \text{cm}^{-3}$, crossing zero between 75 K and 80 K, in agreement with a previous study on the Lifshitz transition [19]. The temperature evolution of the carrier density n is shown in the inset of Fig. 2(a).

We note that the calculated σ_{AHE} in our model uses the chemical potential as the only adjustable parameter, while all other parameters use the values reported in the

literature: $g = 21.3$ [16], the gap is 12 meV [4], the x , y and z Fermi velocities are 9.7×10^5 m/s, 6.8×10^5 m/s and 9.7×10^4 m/s [8], respectively, and relevant lattice constants [1]. Near the Lifshitz transition (e.g. 80 K and 75 K), we found that the Fermi level positioned at 3 meV above or below the gap produces a temperature and magnetic field dependence of σ^{xy} that is in good quantitative agreement with the experimental data. As such, the calculated anomalous conductivity σ_{AHE} should be understood as a model prediction, not as a fitting of the data. The discrepancy between the calculation and the data at 80 K (Fig. 3c) is noted. Quadratic terms in a $k \cdot p$ model become particularly important when the Fermi level is close to the edge of the bands; however, our model does not include these terms. Moreover, as we discuss below, the Lifshitz transition may be accompanied by a topological phase transition. In this case, band inversion is expected in the system [1], which is not captured by the simple $k \cdot p$ model used here. Other band parameters such as the mass and band velocities are possibly renormalized with temperature [20], which was also not accounted for in our model. All these factors can contribute to the discrepancy between our model and the experimental data at temperatures very close to the Lifshitz transition as seen in Fig. 3 (c, f). Nevertheless, this approach properly captures the dominant factors that explain the source of the AHE, its strength, its magnetic field dependence, and how it becomes more pronounced at the Lifshitz transition. These aspects can be traced back to the Berry curvature at the Dirac point and the nodal line structure of ZrTe₅. Similarly, this model can be applied to ZrTe₅ samples with different T_p and/or gap size, as shown in [29], as well as to other Dirac semimetals with large Zeeman splitting.

Our analysis also shows that, while σ_{orb}^{xy} changes sign at T_p , σ_{AHE} does not. The application of the $k \cdot p$ model then requires the use of different signs for the mass term, i.e. $m < 0$ for $T < T_p$ and $m > 0$ for $T > T_p$. The $k \cdot p$ models describing the system above and below the transition cannot be continuously connected without closing the gap. The necessity of this sign change to explain the experimental data indicates the Lifshitz transition involves a change in band topology, not just a simple renormalization of the Fermi level. It means that the system goes through a temperature driven topological phase transition between weak and strong topological insulator as suggested in previous studies [7, 21]. In particular, the sign change of the mass term can be induced by many modes of small atomic displacement that preserve the crystal symmetry [1]. We leave this for future studies.

In summary, we have developed an effective low energy model that treats the classical orbital and the Berry curvature induced anomalous contributions to Hall effects on an equal footing in topological semimetals with a large Landé g -factor. With the input of the materials' electronic and structural parameters, the model can predict

each contribution over a wide range of temperature and magnetic field. It is shown that the model-calculated temperature and magnetic field dependence of the Hall conductivity are in quantitative agreement with the experimental data in ZrTe₅ having a temperature induced Lifshitz transition. We also discovered that a sign change in the mass term in our calculations is involved as the system goes through the Lifshitz transition. It would be interesting to investigate whether the sign changing is the result of topological phase transition in the electronic structures that coexists with the Lifshitz transition and in particular a subtle structural transition.

ACKNOWLEDGEMENTS

We acknowledge helpful discussions with Alexander Abanov and Jennifer Cano. This work was primarily supported by the U.S. Department of Energy, Office of Basic Energy Sciences, Division of Materials Sciences and Engineering, under Contract No. DE-SC0012704. G.C. was supported by Grant NSF DMR-1606591. This research used resources of the Center for Functional Nanomaterials, which is a U.S. DOE Office of Science Facility, at Brookhaven National Laboratory.

* These authors contributed equally

† qiangli@bnl.gov

- [1] N. Aryal, X. Jin, Q. Li, A. M. Tsvelik, and W. Yin, Topological phase transition and phonon-space Dirac topology surfaces in ZrTe₅, *Phys. Rev. Lett.* **126**, 016401 (2021).
- [2] P. Zhang, R. Noguchi, K. Kuroda, C. Lin, K. Kawaguchi, K. Yaji, A. Harasawa, M. Lippmaa, S. Nie, H. Weng, *et al.*, Observation and control of the weak topological insulator state in ZrTe₅, *Nat. Commun.* **12**, 1 (2021).
- [3] H. Weng, X. Dai, and Z. Fang, Transition-metal pentatelluride ZrTe₅ and HfTe₅: A paradigm for large-gap quantum spin Hall insulators, *Phys. Rev. X* **4**, 011002 (2014).
- [4] Z. G. Chen, R. Y. Chen, R. D. Zhong, J. Schneeloch, C. Zhang, Y. Huang, F. Qu, R. Yu, Q. Li, G. D. Gu, and N. L. Wang, Spectroscopic evidence for bulk-band inversion and three-dimensional massive Dirac fermions in ZrTe₅, *Proc. Nat. Acad. Sci. USA* **114**, 816 (2017).
- [5] J. Mutch, W.-C. Chen, P. Went, T. Qian, I. Z. Wilson, A. Andreev, C.-C. Chen, and J.-H. Chu, Evidence for a strain-tuned topological phase transition in ZrTe₅, *Sci. Adv.* **5**, eaav9771 (2019).
- [6] C. Vaswani, L. L. Wang, D. H. Mudiyansele, Q. Li, P. M. Lozano, G. D. Gu, D. Cheng, B. Song, L. Luo, R. H. J. Kim, C. Huang, Z. Liu, M. Mootz, I. E. Perakis, Y. Yao, K. M. Ho, and J. Wang, Light-driven Raman coherence as a nonthermal route to ultrafast topology switching in a Dirac semimetal, *Phys. Rev. X* **10**, 021013 (2020).
- [7] Z. Fan, Q. F. Liang, Y. B. Chen, S. H. Yao, and J. Zhou,

- Transition between strong and weak topological insulator in ZrTe_5 and HfTe_5 , *Sci. Rep.* **7**, 45667 (2017).
- [8] Q. Li, D. E. Kharzeev, C. Zhang, Y. Huang, I. Pletikosić, A. Fedorov, R. Zhong, J. Schneeloch, G. Gu, and T. Valla, Chiral magnetic effect in ZrTe_5 , *Nat. Phys.* **12**, 550 (2016).
- [9] F. Tang, Y. Ren, P. Wang, R. Zhong, J. Schneeloch, S. A. Yang, K. Yang, P. A. Lee, G. Gu, Z. Qiao, and L. Zhang, Three-dimensional quantum Hall effect and metal-insulator transition in ZrTe_5 , *Nature* **569**, 537 (2019).
- [10] T. Liang, J. Lin, Q. Gibson, S. Kushwaha, M. Liu, W. Wang, H. Xiong, J. A. Sobota, M. Hashimoto, P. S. Kirchmann, *et al.*, Anomalous Hall effect in ZrTe_5 , *Nat. Phys.* **14**, 451 (2018).
- [11] Y. Liu, H. Wang, H. Fu, J. Ge, Y. Li, C. Xi, J. Zhang, J. Yan, D. Mandrus, B. Yan, *et al.*, Induced anomalous hall effect of massive dirac fermions in ZrTe_5 and HfTe_5 thin flakes, *Phys. Rev. B* **103**, L201110 (2021).
- [12] J. Mutch, X. Ma, C. Wang, P. Malinowski, J. Ayres-Sims, Q. Jiang, Z. Liu, D. Xiao, M. Yankowitz, and J.-H. Chu, Abrupt switching of the anomalous Hall effect by field-rotation in nonmagnetic ZrTe_5 , *arXiv preprint arXiv:2101.02681* (2021).
- [13] L. Luo, D. Cheng, B. Song, L.-L. Wang, C. Vaswani, P. M. Lozano, G. Gu, C. Huang, R. H. Kim, Z. Liu, *et al.*, A light-induced phononic symmetry switch and giant dissipationless topological photocurrent in ZrTe_5 , *Nat. Mater.* **20**, 329 (2021).
- [14] N. Nagaosa, J. Sinova, S. Onoda, A. H. MacDonald, and N. P. Ong, Anomalous Hall effect, *Rev. Mod. Phys.* **82**, 1539 (2010).
- [15] R. Karplus and J. M. Luttinger, Hall effect in ferromagnetics, *Phys. Rev.* **95**, 1154 (1954).
- [16] Y. Liu, X. Yuan, C. Zhang, Z. Jin, A. Narayan, C. Luo, Z. Chen, L. Yang, J. Zou, X. Wu, S. Sanvito, Z. Xia, L. Li, Z. Wang, and F. Xiu, Zeeman splitting and dynamical mass generation in Dirac semimetal ZrTe_5 , *Nat. Commun.* **7**, 12516 (2016).
- [17] Y. Choi, J. W. Villanova, and K. Park, Zeeman-splitting-induced topological nodal structure and anomalous Hall conductivity in ZrTe_5 , *Phys. Rev. B* **101**, 035105 (2020).
- [18] Z. Sun, Z. Cao, J. Cui, C. Zhu, D. Ma, H. Wang, W. Zhuo, Z. Cheng, Z. Wang, X. Wan, *et al.*, Large zeeman splitting induced anomalous Hall effect in ZrTe_5 , *npj Quantum Mater.* **5**, 1 (2020).
- [19] H. Chi, C. Zhang, G. Gu, D. E. Kharzeev, X. Dai, and Q. Li, Lifshitz transition mediated electronic transport anomaly in bulk ZrTe_5 , *New J. Phys.* **19** (2017).
- [20] B. Fu, H.-W. Wang, and S.-Q. Shen, Dirac polarons and resistivity anomaly in ZrTe_5 and HfTe_5 , *Phys. Rev. Lett.* **125**, 256601 (2020).
- [21] B. Xu, L. X. Zhao, P. Marsik, E. Sheveleva, F. Lyzwa, Y. M. Dai, G. F. Chen, X. G. Qiu, and C. Bernhard, Temperature-driven topological phase transition and intermediate Dirac semimetal phase in ZrTe_5 , *Phys. Rev. Lett.* **121**, 187401 (2018).
- [22] S. Okada, T. Sambongi, and M. Ido, Giant resistivity anomaly in ZrTe_5 , *J. Phys. Soc. Jpn.* **49**, 839 (1980).
- [23] T. Jones, W. Fuller, T. Wieting, and F. Levy, Thermoelectric power of HfTe_5 and ZrTe_5 , *Solid State Commun.* **42**, 793 (1982).
- [24] T. M. Tritt, N. D. Lowhorn, R. T. Littleton, A. Pope, C. R. Feger, and J. W. Kolis, Large enhancement of the resistive anomaly in the pentatelluride materials HfTe_5 and ZrTe_5 with applied magnetic field, *Phys. Rev. B* **60**, 7816 (1999).
- [25] Y. Zhang, C. Wang, L. Yu, G. Liu, A. Liang, J. Huang, S. Nie, X. Sun, Y. Zhang, B. Shen, *et al.*, Electronic evidence of temperature-induced lifshitz transition and topological nature in ZrTe_5 , *Nat. Commun.* **8**, 1 (2017).
- [26] G. Zheng, J. Lu, X. Zhu, W. Ning, Y. Han, H. Zhang, J. Zhang, C. Xi, J. Yang, H. Du, K. Yang, Y. Zhang, and M. Tian, Transport evidence for the three-dimensional Dirac semimetal phase in ZrTe_5 , *Phys. Rev. B* **93**, 115414 (2016).
- [27] A. Pariari and P. Mandal, Coexistence of topological Dirac fermions on the surface and three-dimensional Dirac cone state in the bulk of ZrTe_5 single crystal, *Sci. Rep.* **7**, 1 (2017).
- [28] Y. Tian, N. Ghassemi, and J. H. Ross, Dirac electron behavior and NMR evidence for topological band inversion in ZrTe_5 , *Phys. Rev. B* **100**, 165149 (2019).
- [29] See supplementary information, which includes Refs. [4, 8, 9, 11, 12, 19, 32–35].
- [30] Here, it is assumed that $2\rho_{xx} \sim \rho_{yy}$, as shown in a number of recent works [11, 12].
- [31] A. Pippard, *Magnetoresistance in Metals*, Cambridge Studies in Low Temperature Physics (Cambridge University Press, 1989).
- [32] R. Y. Chen, Z. G. Chen, X. Y. Song, J. A. Schneeloch, G. D. Gu, F. Wang, and N. L. Wang, Magnetoinfrared spectroscopy of Landau levels and Zeeman splitting of three-dimensional massless Dirac fermions in ZrTe_5 , *Phys. Rev. Lett.* **115**, 176404 (2015).
- [33] G. M. Monteiro, A. G. Abanov, and D. E. Kharzeev, Magnetotransport in Dirac metals: Chiral magnetic effect and quantum oscillations, *Phys. Rev. B* **92**, 165109 (2015).
- [34] P. Shahi, D. J. Singh, J. P. Sun, L. X. Zhao, G. F. Chen, Y. Y. Lv, J. Li, J. Q. Yan, D. G. Mandrus, and J. G. Cheng, Bipolar conduction as the possible origin of the electronic transition in pentatellurides: Metallic vs Semiconducting Behavior, *Phys. Rev. X* **8**, 021055 (2018).
- [35] E. Martino, I. Crassee, G. Eguchi, D. Santos-Cottin, R. D. Zhong, G. D. Gu, H. Berger, Z. Rukelj, M. Orlita, C. C. Homes, and A. Akrap, Two-dimensional conical dispersion in ZrTe_5 evidenced by optical spectroscopy, *Phys. Rev. Lett.* **122**, 217402 (2019).